Available online at www.sciencedirect.com
SCIENCE DIRECT®
Earth and Planetary Science Letters 222 (2004) 145–160
EPSL
www.elsevier.com/locate/epsl

Determining the cooling history of in situ lower oceanic crust—Atlantis Bank, SW Indian Ridge

Barbara E. John[a,*], David A. Foster[b], John M. Murphy[a], Michael J. Cheadle[a], A. Graham Baines[a], C. Mark Fanning[c], Peter Copeland[d]

[a] *Department of Geology and Geophysics, University of Wyoming, Laramie, WY 82071, USA*
[b] *Department of Geological Sciences, University of Florida, PO Box 112120, Gainesville, FL 32611, USA*
[c] *Research School of Earth Sciences, Australian National University, Canberra, ACT 0200, Australia*
[d] *Department of Geosciences, University of Houston, Houston, TX 77204-5503, USA*

Received 3 July 2003; received in revised form 4 September 2003; accepted 10 February 2004

Abstract

The cooling history and therefore thermal structure of oceanic lithosphere in slow-spreading environments is, to date, poorly constrained. Application of thermochronometric techniques to rocks from the very slow spreading SW Indian Ridge provide for the first time a direct measure of the age and thermal history of in situ lower oceanic crust. Crystallization of felsic veins (~850°C) drilled in Hole 735B is estimated at 11.93±0.14 Ma, based on U–Pb analyses of zircon by ion probe. This crystallization age is older than the 'crustal age' from remanence inferred from both sea surface and near-bottom magnetic anomaly data gathered over Hole 735B which indicate magnetization between major normal polarity chrons C5n.2n and C5An.1n (10.949–11.935 Ma). $^{40}Ar/^{39}Ar$ analyses of biotite give plateau ages between 11 and 12 Ma (mean 11.42±0.21 Ma), implying cooling rates of >800°C/m.y. over the first 500,00 years to temperatures below ~330–400°C. Fission-track ages on zircon (mean 9.35±1.2 Ma) and apatite reveal less rapid cooling to <110°C by ~7 Ma, some 4–5 m.y. off axis.

Comprehensive thermochronometric data from the structurally intact block of gabbro between ~700 and 1100 m below sea floor suggest that crust traversed by ODP Hole 735B mimics conductive cooling over the temperature range ~900–330°C, characteristic of a 2-D plate-cooling model for oceanic lithosphere. In contrast, lower temperature chronometers (fission track on zircon, titanite, and apatite; $T \leq 280$°C) are not consistent with these predictions and record anomalously high temperatures for crust >700 m below sea floor at 8–10 Ma (i.e. 2–4 m.y. off axis). We offer two hypotheses for this thermal anomaly:

(i) Off-axis (or asymmetric) magmatism that caused anomalous reheating of the crust preserved in Hole 735B. This postulated magmatic event might be a consequence of the transtension, which affected the Atlantis II transform from ~19.5 to 7.5 Ma.
(ii) Late detachment faulting, which led to significant crustal denudation (2.5–3 km removed), further from the ridge axis than conventionally thought.

Keywords: Ocean Drilling Program Site 735B; cooling; lower oceanic crust; thermochronometry

* Corresponding author. Tel.: +1-307-766-4232; fax: +1-307-766-6679.
E-mail address: bjohn@uwyo.edu (B.E. John).

0012-821X/$ - see front matter © 2004 Elsevier B.V. All rights reserved.
doi:10.1016/j.epsl.2004.02.014

1. Introduction

The thermal evolution of oceanic crust fundamentally reflects the processes of both crustal and lithospheric growth. Modeling studies estimate that submarine hydrothermal systems remove ~30% of the heat lost from oceanic crust [1,2]. 'Snapshot' measurements of vent fluids emanating from active hydrothermal systems at ridge axes give some idea of active heat loss over very short time scales and perhaps restricted areas. In contrast to the wealth of modeling and in situ measurements of vent fluids emanating from active hydrothermal systems, very little data exist for the time-averaged (or mean) thermal history of in situ lower oceanic crust [3]. This is due at least in part to a lack of appropriate samples and the inherent difficulty in obtaining this information. In this paper, we combine geo- and thermochronometric methods to define the timing and rates of protracted heat loss (from emplacement to denudation, $\sim 850\,^{\circ}\mathrm{C} \leq T \leq 100\,^{\circ}\mathrm{C}$) of oceanic crust at the very slow spreading SW Indian Ridge.

Thermochronometry, the application of temperature-sensitive rock dating techniques to the reconstruction of rock thermal histories, has been dominated by $^{40}Ar/^{39}Ar$ and fission-track dating methods on continental rocks. In igneous systems, moderate subsolidus temperatures (~150–≥500 °C) are accessible with argon ($^{40}Ar/^{39}Ar$) analysis of various potassium-bearing minerals [4]. Fission-track (FT) dating is particularly useful in thermal history studies at relatively low temperature, below about 110 °C using apatite [5], and up to ~240–280 °C using titanite and zircon [6,7]. Integration of these techniques, together with the uranium–lead (U–Pb) system applied to zircon to attain crystallization ages for igneous bodies, allows details of both the thermal and tectonic evolution of rock bodies over a range in temperature from magmatic to low-temperature subsolidus conditions (≤900 to below 100 °C). One problem in using these techniques for oceanic crust, however, is that the major constituents of basalt and gabbro are olivine, clinopyroxene, and plagioclase, none of which contain significant concentrations of either potassium or uranium. However, recent advances in the development of high-precision dating techniques allow the dating of single zircon, sphene, and/or apatite crystals found as trace minerals in rocks such as gabbronorites, oxide gabbros, and felsic veins in ocean crust.

Isotopic systems have been used as thermochronometers for rocks in regions of extreme crustal extension in continental settings ([8] and references therein). To date, however, no comprehensive study has been completed for oceanic lithosphere. In this paper, we present uranium–lead (U–Pb), argon ($^{40}Ar/^{39}Ar$), and fission-track (FT) data from a spectrum of minerals hosted by late-stage felsic vein material recovered from Hole 735B during ODP Legs 118 and 176. The samples span much of the >1500 m of oceanic layer 3 drilled and therefore provide a vertical section through a significant thickness of the lower oceanic crust. The thermochronometric study of these samples provides, for the first time, the opportunity to document the in situ thermal history of lower crust generated in a very slow spreading environment. Specifically, these data provide important constraints on the thermal and mechanical structure of the crust after magma emplacement and allow determination of cooling rates associated with amagmatic extension.

1.1. Location and tectonic setting of Atlantis Bank and Hole 735B

The slow-spreading SW Indian Ridge (SWIR) separates the African and Antarctic plates and extends for nearly 8000 km (Fig. 1). Atlantis Bank is the best studied region of the SWIR and comprises an uplifted and denuded block of lower oceanic crust and upper mantle that formed ~12 Ma, as an inside corner high at the intersection of the Atlantis II transform and the ridge to the north. Estimated spreading rates for this segment of the asymmetric, very slow spreading ridge are ~8.5 and 5.5 mm/year on the Antarctic and African plates, respectively [9]. ODP Hole 735B (32°43.392′S, 57°15.960′E) was drilled on the crest of the transform ridge that forms the eastern wall of the Atlantis II fracture zone, ~93 km south of the present-day SWIR axis (Fig. 1). The drill site at roughly 720-m water depth is located on the top of Atlantis Bank, a subhorizontal, bathymetric high, ~4 km east–west and greater than 9 km in the north–south direction parallel to the spreading direction.

Combined drilling, dredging, ROV, and submersible observations indicate that Atlantis Bank exposes variably foliated, lower oceanic crust (seismic Layer 3), of predominately gabbroic composition, and upper

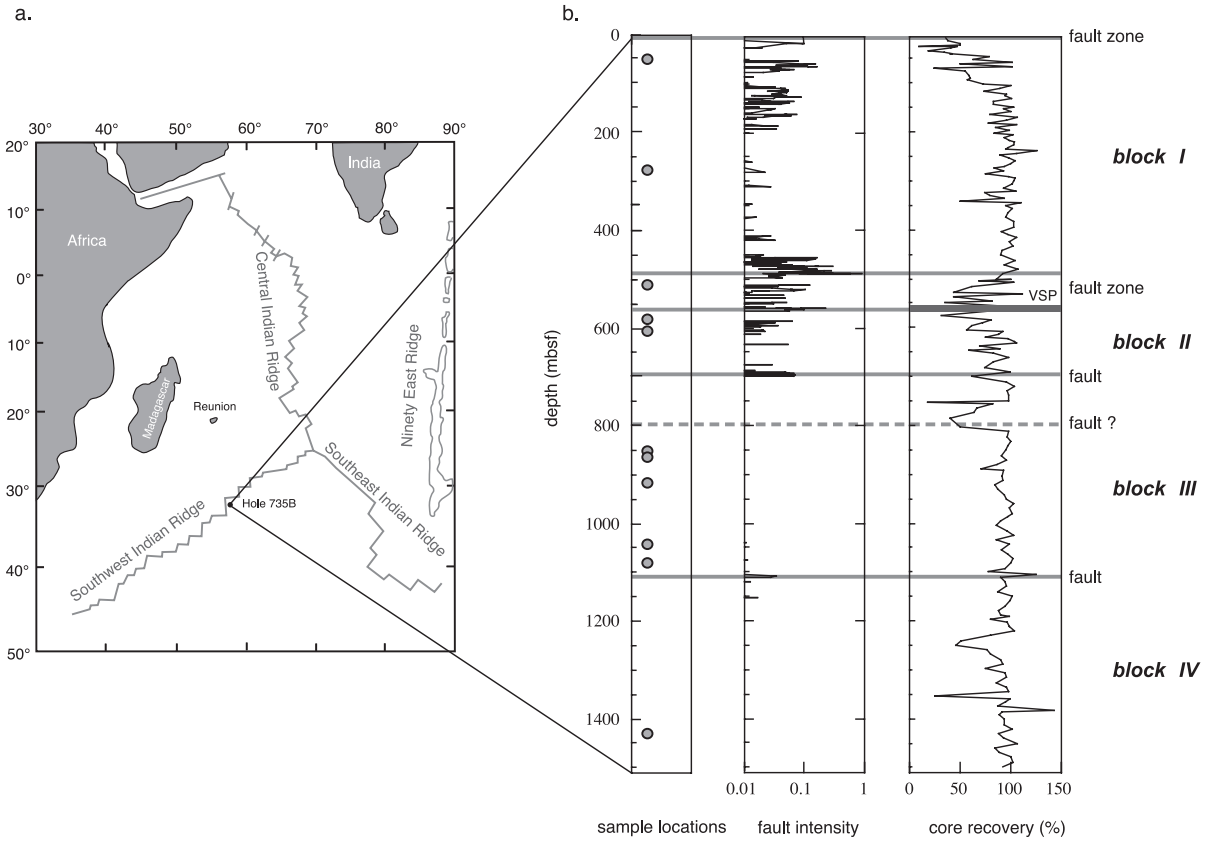

Fig. 1. (a) Location of Hole 735B along the very slow spreading SW Indian Ridge, southern Indian Ocean. (b) Brittle features and sample locations in ODP Hole 735B–SW Indian Ridge (modified from [12]). Brittle deformation is localized along faults at ~490, 560, and 690–700 mbsf, with minor zones at 1076 and 1100–1120 mbsf. These faults separate the core into a minimum of four structural blocks (I–IV). The faults at 490, 560, and 690–700 mbsf overprint granulite and amphibolite grade shear zones and may represent long-lived brittle–ductile shear zones with significant displacement. The top of the hole and Atlantis Bank is interpreted as an eroded detachment fault surface.

mantle [10–13]. These observations support the hypothesis that Atlantis Bank is an oceanic core complex mantled by a long-lived normal or detachment fault system along which up to 2.4 km of upper crust was tectonically removed [13,14]. About 90% of the platform gabbro shows moderate to intense crystal-plastic, semi-brittle, and cataclastic deformation, in contrast to less than a quarter of the Hole 735B gabbros, consistent with the interpretation that the gently dipping domed surface of Atlantis Bank, above ~2500 m, is a faulted, slightly eroded footwall to a major low-angle normal or detachment fault system [11,12,15].

Hole 735B penetrated 1508 m of gabbroic lower crust [12]. The complex igneous stratigraphy documented in the hole is interpreted as three series or suites of olivine gabbro and allied troctolites, together with related oxide gabbros and felsic veins of more differentiated compositions [13]. Together, the olivine gabbro suites comprise ~76% of Hole 735B; the more fractionated oxide gabbro and felsic veins comprise the remaining 24%. Oxide gabbros and veins occur throughout the core, but are concentrated in the upper 1100 m [12,15] and at the surface of Atlantis Bank. The oxide gabbros are late-stage, fractionated melts derived from the olivine gabbros, and the felsic veins are the end product of magmatic differentiation [13]. Thus, these rocks are the final crystallization products of ‘crust-forming’ magmas. The veins form small pockets or dikes centimeters in width (Fig. 2) and are characterized by medium-to-coarse-grained euhedral plagioclase±clinopyroxene±

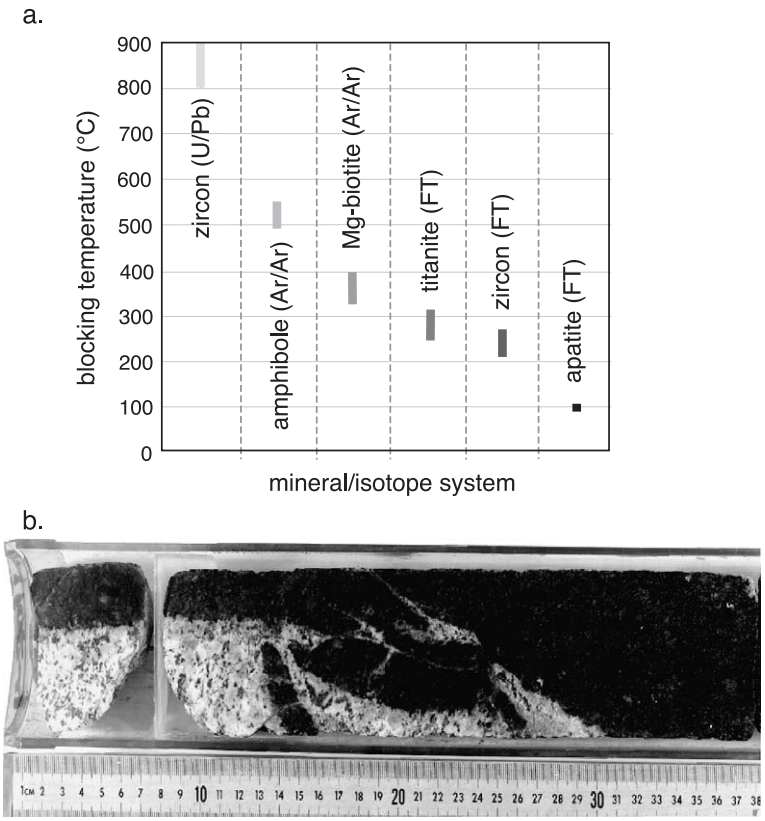

Fig. 2. (a) Compilation of estimated closure and/or blocking temperatures for minerals and thermochronometric systems used in this study. Amphibole and biotite show an extended range in closure temperature for the argon system due to high Mg contents in biotite, and the very rapid cooling rates estimated for Hole 735B. Details of estimated closure temperatures for rapid cooling rates (>100 to 1000°C/m.y.) are discussed in the text. (b) Undeformed felsic vein network such as those sampled for this study (with amphibole, biotite titanite, zircon, and apatite), cutting fresh olivine gabbro sampled from 637.4 mbsf (ODP 176-735B-110R-4, 1–38).

biotite±amphibole±alkali feldspar±quartz± magnetite. Most importantly, these in situ strongly fractionated rocks are also host to the trace minerals zircon, titanite, and apatite, which will be used in the thermo-chronometry discussed below.

Metamorphism and hydrothermal alteration of Hole 735B cores has been characterized in three stages: initial granulite to amphibolite facies alteration under dynamic conditions, followed by greenschist facies alteration associated with uplift and denudation [12,13]. This was followed by lower temperature, static alteration, associated with block uplift and subsequent cooling to the present day. Overall, rocks recovered from Hole 735B have suffered limited alteration. The most intensely altered part of the core is between 500 and 600 mbsf, where both amphibole and secondary plagioclase are most abundant and primary minerals are 10–40% replaced. In contrast, the Leg 118 Shipboard Science Party [10] noted that the amphibolite grade mylonites at the top of the hole and common across Atlantis Bank exhibit alteration, locally up to 100% [16,17]. Fluid inclusion studies [14] indicate that rocks from the lower half of Hole 735B show little hydrothermal alteration, which Kelley and Früh-Green interpret as indicating a very low contribution from convective cooling below ~800-m depth.

Macroscopic deformation in Hole 735B is localized in discrete shear zones and faults, with the bulk of the core (77%) not deformed [12]. Brittle fracture density as proxied by fault intensity and recovered fault rocks, as well as hydrothermal vein intensity,

decreases down hole. Discrete planar faults with associated gouge, breccia, cataclasite, and ultracataclasite cut all rock types and are associated with brittle and semi-brittle deformation. Faults and associated cataclastic deformation in the hole are concentrated in the top 50% of the hole (to ~720 mbsf) and are virtually absent below approximately 1400 m. Fault rocks of all intensities were recovered, including gouge, breccia, and oxide-rich cataclasite and ultracataclasite. Indicators of the existence of faults not recovered include brecciated fragments and rubble with slickensided striae.

Of significance to this study are the dominantly low-temperature, cataclastic fabrics defining discrete faults and zones of associated cataclasis shown in Fig. 1. Based on thickness and fracture intensity of recovered cataclastic rocks, brittle deformation is localized along faults at the sea floor, at ~490 mbsf (with several minor zones between ~460 and 495 mbsf), at ~560 and at 690–700 mbsf, marked by relatively low core recovery (<60%), and within several minor zones of fracturing/cataclasis around 1100 mbsf. Deformation intensity at the top of Hole 735B and the platform making up Atlantis Bank is high; the bank itself is considered a slightly eroded low-angle normal or detachment fault surface [John, unpublished submersible observations, 1998, 2002; 12,13]. The region between 460 and 570 mbsf is considered to be an ~100-m-thick fault zone, bound below by the principle slip surface(s) at ~560 mbsf. Down hole logging data from Leg 176 suggest that there are two faults centered at 555 and 565 mbsf, 2–4 m thick, respectively. The logs indicate reduced velocity, density, resistivity, and elevated porosity at these intervals [12], and correlate with the approximate depth of a seismic reflector identified during the Leg 118 VSP experiment [18]. The second, deeper VSP reflector at 760–825 mbsf cannot be correlated with anything in the core, but core recovery was <50% over this interval (Fig. 1). These brittle faults overprint granulite and amphibolite grade shear zones and were active at greenschist- and sub-greenschist facies conditions. They divide the section into four (I–IV) structural blocks [Block I (0–460 mbsf), Block II (570–700 mbsf), Block III (700–1100 mbsf), and Block IV (1100 mbsf–below the bottom of the hole)] and represent long-lived brittle–ductile shear zones. Blocks III and IV are characterized by very low fracture density and limited alteration: data from Block III are therefore used in the thermal modeling discussed below. Sampled felsic veins used in this study are shown as circles in Fig. 1.

1.2. Previous age estimates for the crust at 735B

Previous estimates of the age of crust at the site on Atlantis Bank hosting Hole 735B include both marine magnetic anomaly and U–Pb zircon data. Preliminary U–Pb zircon dating gave an estimated crustal age of 11.3 Ma (no errors quoted) [16]. Estimates of crustal age based on marine magnetic anomalies are somewhat confused in the literature, but suggest that the crust beneath Hole 735B lies in the age range from ~11.5 to 11.8 Ma. Dick et al. [10] interpreted 735B to lie within sea-surface magnetic anomaly 5r; based on the revised time scale of Cande and Kent [19], this is between 10.949 and 11.935 Ma. A revised estimate of the age of Hole 735B comes from Dick et al. [12] who indicate again based on sea-surface data that the hole was drilled in rocks magnetized during anomaly 5r.2n or 11.5 Ma. A recent detailed deep-tow magnetic survey [20] confirms that Hole 735B was drilled between chrons c5n.2n and C5An, bracketing the age between 11.531 and 11.935 Ma. The hole was drilled ~3 km south of the southern boundary of anomaly C5r.2n, indicating magnetization slightly older than the anomaly (11.476–11.531 Ma). Based on location of picked anomalies from the deep-tow data [20], a uniform spreading rate, and the hole position, an additional estimate of the magnetic age at Hole 735B is ~11.75 Ma.

2. Cooling and denudation history

The cooling and denudation history recorded in rocks from Hole 735B are determined using a variety of established methods. The isotope systems used as thermochronometers in this study include U–Pb, $^{40}Ar/^{39}Ar$, and fission-track dating. These radioactive systems, as applied to a variety of minerals (Fig. 2), define a set of closure or annealing temperatures ranging from magmatic (≥850 °C) to subsolidus conditions (<110 °C). These results are compared with the estimated sea surface and deep-tow magnetic anomaly ages [19,20]. For ease in referencing, all samples

discussed in the text are numbered based on their collection depth in Hole 735B (i.e. sample #606 is from 606 m below sea floor and correlates to core ODP-176-735B-104R-3, 5–9 cm).

2.1. Sample preparation

Eighteen samples of felsic veins were collected from Hole 735B, where sufficient material was available (Figs. 1 and 2). All samples were initially between 7 and 30 cm^3, with mean sample volume 17 cm^3. Mineral separation was completed after hand crushing with agate mortar and pestle using a FRANZ magnetic separator and heavy liquids. Based on microscopic observation of initial separates, 11 of the 18 samples yielded useable minerals of sufficient volume for analysis. These separates of zircon, apatite, and titanite were handpicked to greater than 99% purity. Approximately 25 μg of amphibole and between 10 and 20 μg of biotite and potassium feldspar were handpicked for $^{40}Ar/^{39}Ar$ analyses. Some of the samples of amphibole and biotite were difficult to pick to satisfactory purity, as the majority of each had innumerable inclusions, and were therefore not analyzed.

2.2. U–Pb analyses

2.2.1. Analytical methods

Zircon was separated from sample #606 (ODP 176-735B-104R-3, 5–9 cm), an undeformed, medium-grained, hornblende-biotite granodiorite vein that cuts foliated gabbro. The separated zircon population is varied in size, color, and shape (euhedral to subhedral, with variable aspect ratios). Data presented are from the ion-microprobe analyses of these individual zircon grains. Analytical procedures for defining precise U–Pb ages from relatively young zircons using SHRIMP-II are described by Compston et al. [21] and Williams [22]. Methods similar to these were applied in this study except that the reference zircon used was AS3 from the Duluth gabbro. The Duluth gabbro reference zircon allows considerably better accuracy and precision than the previous standard SL13 [22]. Correction for common Pb in the zircons was made using the measured $^{207}Pb/^{206}Pb$ and $^{238}U/^{206}Pb$ ratios following Tera and Wasserburg [23]. The overall uncertainty in the calculated age is approximately 1% for the $^{238}U/^{206}Pb$ age. Closure temperatures associated with U–Pb systematics in zircon are estimated at between 800 and 900 °C [24] for rocks of granodiorite composition.

2.2.2. U–Pb results

The uncorrected U–Pb results are shown plotted on a Tera–Wasserburg diagram in Fig. 3 and tabulated in Table 1. The 15 spot analyses group tightly just above concordia due to very minor common Pb and give a well-defined weighted mean age of 11.93 ± 0.14 (2σ) Ma for the entire population of zircons analyzed. This age is interpreted to be the time of crystallization of the vein that intrudes the gabbro. The occurrence of minor common Pb recorded by these zircons is suspected to be the result of seawater infiltration at high temperature. The common Pb in these zircons, however, results in an insignificant age correction for the analyses (±1%).

2.3. $^{40}Ar/^{39}Ar$ analyses

2.3.1. Analytical methods

$^{40}Ar/^{39}Ar$ analyses were performed at the University of Houston using the methods summarized in Spell et al. [25]. Four biotite and two hornblende separates were analyzed by step heating. The remaining four hornblende and one biotite separates were degassed in a single fusion step due to the very low gas yields arising from the low K_2O concentrations in the amphibole and the very small volume of biotite in sample 571. Age spectra for these biotite analyses are shown in Fig. 4; isotopic results for all biotite and hornblende analyzed are summarized in Table 2 for completeness.

2.3.2. Ar/Ar results

Inferences about the intermediate temperature thermal history of samples from Hole 753B are made from the form of $^{40}Ar/^{39}Ar$ age spectra [4]. During cooling following crystallization, closure temperatures for argon in hornblende and biotite are normally taken to be between 550 and 490 °C [25] and between 350 and 280 °C [26], respectively, for cooling rates between 5 and 100 °C/m.y. Revised estimates of closure temperatures based on mineral composition and cooling rate were calculated for biotite (365±35 °C) using methods outlined

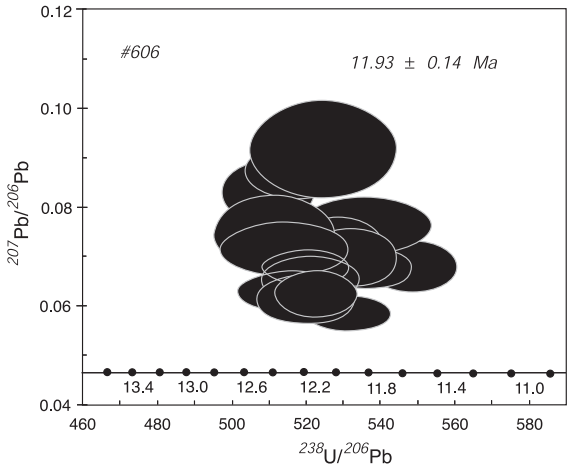

Fig. 3. Emplacement age ($T \sim 850 \pm 50$ °C): U–Pb zircon (SHRIMP II) results for sample #606 (ODP 176-735B-104R-3, 5–9 cm). Tera–Wasserburg plot of 15 spot analyses for zircon in a granodioritic vein cutting foliated gabbro. Data-point error ellipses $\pm 1\sigma$; calculated weighted mean of age, 2σ.

in [4] and microprobe mineral compositions from analyzed felsic vein material (Robinson, personal communication, 2001).

Age spectra from biotite samples 851, 865, and 1040 exhibit well-defined plateau segments with ages of 11.46±0.30, 11.89±0.38, and 11.13±0.40 Ma, respectively (2σ errors). Biotite from sample 938 yielded a more discordant age spectrum with a total gas age of 11.20±0.60 Ma. Biotite from sample 571 gave a total fusion age of 13.95±4.92 Ma.

Mineral data from analyzed biotite show a range in Mg composition between 10.5 and 15.1 wt.% MgO and K_2O from 8.5 to 9.1 wt.%. These Mg concentrations are typical of biotite with high closure temperatures, ~330–400 °C [4]. Well-defined plateau ages for biotite from samples 851, 865, and 1040 record cooling through this temperature range. The two samples at 851 and 865 mbsf give concordant ages and cooled at the same time. The difference in age between these two samples and 1040 may be significant and is possibly due to the samples from greater depths in the hole reaching biotite closure at younger times. The minor discordance in the spectrum of biotite in sample 938 could indicate that the sample lost a small fraction of radiogenic ^{40}Ar after cooling through biotite closure. The fact that the total fusion age for sample 938, however, lies between the ages of 1040 and 851 suggests that this is not significant. The total fusion age for 571 biotite is concordant with the other ages owing to its very large error. The mean biotite cooling age for Block III is 11.42±0.21 Ma.

Table 1
SHRIMP U–Pb zircon results for sample 606 (ODP 176-735B-104R-3, 5–9 cm)

Grain spot	U (ppm)	Th (ppm)	Th/U	Pb* (ppm)	$^{204}Pb/^{206}Pb$	f_{206} (%)	Total				Radiogenic		Age (Ma)	
							$^{238}U/^{206}Pb$	±	$^{207}Pb/^{206}Pb$	±	$^{206}Pb/^{238}U$	±	$^{206}Pb/^{238}U$	±
1.1	296	171	0.58	1	0.011344	3.79	535.6	14.5	0.0761	0.0047	0.00180	0.00005	11.6	0.3
2.1	516	243	0.47	1	0.005460	2.76	548.4	9.8	0.0680	0.0043	0.00177	0.00003	11.4	0.2
3.1	535	225	0.42	1	0.005228	2.04	522.6	9.0	0.0623	0.0038	0.00187	0.00003	12.1	0.2
4.1	378	203	0.54	1	0.001711	2.97	531.8	10.4	0.0696	0.0048	0.00182	0.00004	11.8	0.2
5.1	402	221	0.55	1	0.000091	3.22	528.2	10.2	0.0716	0.0052	0.00183	0.00004	11.8	0.2
6.1	704	456	0.65	2	–	1.55	531.2	9.5	0.0585	0.0029	0.00185	0.00003	11.9	0.2
7.1	300	136	0.46	1	0.002183	5.23	517.5	11.4	0.0875	0.0047	0.00183	0.00004	11.8	0.3
8.1	485	347	0.72	1	0.000813	1.91	519.9	10.8	0.0613	0.0040	0.00189	0.00004	12.2	0.3
9.1	281	143	0.51	1	0.000177	5.78	524.6	16.1	0.0917	0.0081	0.00180	0.00006	11.6	0.4
10.1	269	154	0.57	1	0.005046	3.19	514.1	14.1	0.0714	0.0045	0.00188	0.00005	12.1	0.3
11.1	341	167	0.49	1	0.004256	4.70	510.0	10.1	0.0832	0.0051	0.00187	0.00004	12.0	0.3
12.1	471	274	0.58	1	0.005045	2.71	536.6	9.7	0.0676	0.0033	0.00181	0.00003	11.7	0.2
13.1	385	170	0.44	1	0.001501	2.40	521.2	10.8	0.0652	0.0040	0.00187	0.00004	12.1	0.3
14.1	509	315	0.62	1	0.000010	2.11	515.5	11.4	0.0629	0.0031	0.00190	0.00004	12.2	0.3
15.1	291	151	0.52	1	0.003466	3.59	511.2	13.0	0.0745	0.0065	0.00189	0.00005	12.2	0.3

(1) Uncertainties given at the 1σ level. (2) f_{206} % Denotes the percentage of ^{206}Pb that is common Pb. (3) Correction for common Pb made using the measured $^{238}U/^{206}Pb$ and $^{207}Pb/^{206}Pb$ ratios following Tera and Wasserburg [23], as outlined in Compston et al. [21].

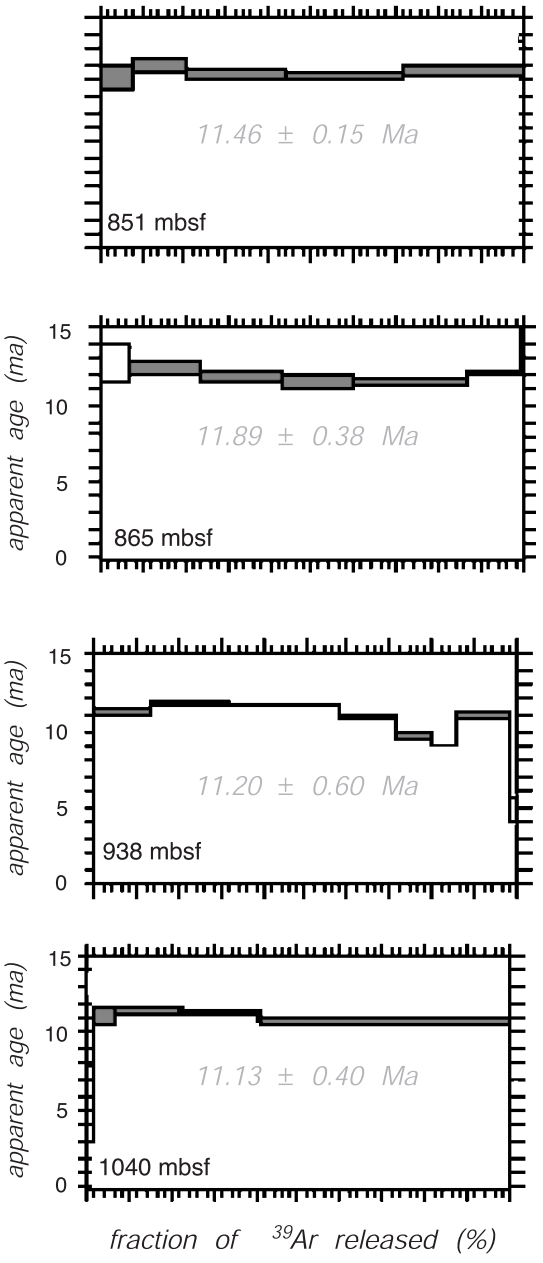

Fig. 4. Argon release spectra for biotite samples from ODP Hole 735B. Errors shown on argon release diagram are $\pm 1\sigma$, as discussed in the text, and given in Table 2. Reported plateau ages are given with 2σ errors. Biotite shows good plateaus with concordant ages down hole, indicative of rapid cooling below ~365°C.

Using this cooling age in combination with the U–Pb crystallization age implies an average cooling rate of ~800°C/m.y. for the first 500,000 years of cooling off axis.

Integrated ages from hornblende separates are more discordant than the biotite results. Total fusion ages for samples 53, 581, 517, and 865 range from about 7.8 to 9.8 Ma. Analysis of sample 1040 hornblende yields relatively old ages in the first two steps and a plateau age of 12.8±1.2 Ma for ~90% of the gas released. A single step from sample 297 gave an age of about 14.7 Ma. The disturbance of the hornblende data and the low bulk K_2O contents suggests extreme caution in trying to date oceanic crust using hornblende. Preliminary microprobe mineral analyses suggest that the younger total fusion ages given by the remaining amphibole separates (53, 517, and 571) are possibly due to overgrowths/intergrowths of actinolite and/or tremolite with the hornblende. These no doubt resulted from moderate- to low-temperature (~200–400°C) hydrothermal fluids influencing the crust near the sample sites. Due to the inherent problems with the amphiboles dated, no hornblende ages are used in either the discussion or calculations of cooling of the lower crust below.

2.4. Fission-track analyses

2.4.1. Analytical methods

Fission-track dating of zircon and titanite provides a thermal record of the host rock at temperatures from 280±40°C (titanite closure interval) [6,26] to less than 240±30°C (zircon closure interval) [7,27]. Fission tracks in apatite grains with Cl concentrations between ~0.1 and 0.4 wt.%, reserve a record of the thermal history of a rock below temperatures of ~110±10°C [5,28–30].

Fission-track analyses of separated zircon and titanite were performed at New Mexico Tech following the procedures described in Fitzgerald and Gleadow [28]. Apatite fission-track age and confined track length distribution analyses followed the techniques outlined in [5] and were performed at the University of Wyoming. Fission-track ages were calculated using the zeta calibration method [31]. Errors were calculated using the conventional method of Green [32], assuming a Poisson distribution.

Table 2
$^{40}Ar/^{39}Ar$ analytical data

Temperature (°C)	Time at temperature	$^{36}Ar/^{39}Ar$	$^{37}Ar/^{39}Ar$	$^{38}Ar/^{39}Ar$	$^{40}Ar/^{39}Ar$	$^{40}Ar^*/^{39}Ar$	Moles ^{39}Ar	% $^{40}Ar^*$	Cum. % ^{39}Ar	Calculated age (Ma±1s)
938 biotite	J=1.270×10^{-3}									
850	8.3	0.0374	0.0118	0.154	15.99	4.9278	1.620e−17	30.9	13.1	11.26±0.47
900	8.1	0.0031	0.0039	0.1284	6.1435	5.1956	2.270e−17	84.9	31.5	11.86±0.47
970	8.2	0.0034	0.0025	0.1238	6.185	5.1536	3.310e−17	83.7	58.2	11.77±0.46
1040	8.9	0.0027	0.0025	0.116	5.6298	4.824	1.640e−17	86.1	71.5	11.02±0.44
1110	9.1	0.0042	0.0053	0.1193	5.5002	4.2492	1.010e−17	77.6	79.7	9.71±0.39
1150	9.1	0.0051	0.0062	0.1406	5.407	3.8642	7.460e−18	71.8	85.7	8.83±0.37
1200	8.5	0.0019	0.021	0.111	5.446	4.8537	1.570e−17	89.6	98.4	11.09±.044
1300	8.9	0.0118	0.1457	0.0923	5.6888	2.1837	1.960e−18	38.6	100	5.00±0.78
851 biotite	J=1.130×10^{-3}									
700	4.1	1.606	0.1053	0.579	490.58	16.0063	2.590e−19	3.3	0.4	32.34±18.29
850	9.2	0.0943	0.0083	0.1917	33.4134	5.532	4.800e−18	16.6	8	11.24±0.96
950	9.1	0.0215	0.0042	0.1616	12.2337	5.8711	7.730e−18	48.1	20.3	11.93±0.69
1050	9.2	0.0152	0.005	0.1549	10.122	5.6042	1.520e−17	55.5	44.5	11.39±0.56
1150	9.4	0.0033	0.0021	0.1442	6.5616	5.5674	1.730e−17	85.2	72.1	11.31±0.54
1400	9.5	0.0021	0.0018	0.1362	6.3491	5.7078	1.750e−17	90.3	100	11.60±0.56
865 biotite	J=1.110×10^{-3}									
700	3.6	0.6302	0.0912	0.1454	216.746	30.5078	1.370e−19	14.1	0.3	60.08±26.40
850	8.3	0.0933	0.0031	0.1468	34.0068	6.4041	2.820e−18	18.8	6.3	12.78±1.35
950	8.5	0.0112	0.0036	0.1192	9.4817	6.1424	8.150e−18	65	23.8	12.26±0.69
1030	8.9	0.0068	0.0074	0.1161	7.9812	5.9496	8.830e−18	74.8	42.8	11.88±0.66
1110	9.3	0.0021	0.0052	0.1143	6.3359	5.7031	7.810e−18	90.4	59.6	11.38±0.67
1170	8.8	0.0011	0.0016	0.1118	6.0889	5.7356	1.280e−17	94.6	87	11.45±0.58
1250	9.1	0.0003	0.003	0.1095	6.1589	6.0503	5.640e−18	98.7	99.1	12.08±0.57
1400	9.3	0.0069	0.0439	0.1148	16.4888	14.4359	4.070e−19	87.7	100	28.68±2.46
1040 biotite	J=1.160×10^{-3}									
650	0	0.913	0	2.2428	380.278	110.539	1.360e−19	29.1	0.1	217.66±43.34
750	8.2	0.4938	0.1407	0.3997	148.458	2.5408	2.470e−18	1.7	1.6	5.31±2.46
850	8.7	0.0498	0.0084	0.1604	20.0042	5.2809	9.270e−18	26.4	7.1	11.02±0.67
950	9	0.0148	0.0065	0.1446	9.8614	5.4637	2.520e−17	55.6	22.2	11.40±0.52
1050	9.3	0.0087	0.0062	0.1339	8.0149	5.4214	3.080e−17	67.9	40.7	11.31±0.50
1400	9.2	0.0027	0.0048	0.1256	5.9359	5.1136	9.890e−17	86.5	100	10.67±0.49
571 biotite	J=1.315×10^{-3}									
1400	10.1	0.0299	0.0858	0.2619	14.5986	5.7481	1.940e−18	39.4	100	13.59±2.46
571 hornblende	J=1.300×10^{-3}									
1250	10.3	0.0425	14.3759	0.4435	14.9641	3.3226	1.090e−17	22	100	7.78±0.45
1040 hornblende	J=1.207×10^{-3}									
900	9	0.6116	1.218	0.4577	212.172	31.5324	2.980e−19	14.8	5.1	67.39±14.65
1000	8.5	0.0764	1.9045	0.1054	35.6569	13.1905	3.810e−19	37	11.5	28.50±9.46
1100	8.7	0.0382	16.9688	0.2416	16.1791	6.0107	3.370e−18	36.7	68.9	13.04±1.24
1500	9.2	0.0353	17.5898	0.2433	14.4031	5.104	1.830e−18	35	100	11.08±2.74
297 hornblende	J=1.225×10^{-3}									
1200	8.7	0.0789	20.0376	0.7998	28.6521	6.6651	7.810e−18	22.9	100	14.67±0.73
53 hornblende	J=1.255×10^{-3}									
1250	10.2	0.2592	46.6032	5.3436	77.3968	3.9821	2.370e−18	5	100	8.99±3.09

($^{39}Ar/^{37}Ar$)Ca=0.00074, ($^{36}Ar/^{37}Ar$)Ca=0.00021, ($^{38}Ar/^{39}Ar$)K=0.01077, ($^{40}Ar/^{39}Ar$)K=0.02622, ($^{40}Ar/^{39}Ar$)K=0.02622.

2.4.2. Fission-track results

2.4.2.1. Titanite and zircon. Within error, all titanite and zircon fission-track ages are the same (Fig. 5). The zircon ages range between 9.1±0.6 (2σ) and 9.7±1.2 Ma, and titanite from 7.4±1.8 (2σ) to 10.2±3.4 Ma (Table 3). However, titanite has low uranium concentrations and hence has larger uncertainties compared to

those for zircon. The 'chi-squared (χ^2)' statistic is used to determine the probability that all grains counted belong to a single population of ages [33], and central ages are reported for all samples [34]. Both the titanite and zircon age populations are consistent with the hypothesis that there is only one age population represented in each sample. However, at least two types of zircon are recognized in samples 920 and 996 (Table 3): one with low uranium concentrations and one with more typical uranium concentrations. The mean of all zircon ages is 9.35±1.2 Ma; when combined with the biotite Ar/Ar, cooling age data suggest average cooling rates of ~45–90°C/m.y. over the range in temperature from ~400 to 200°C. In addition, the similarity of fission-track zircon ages in Blocks II and III (Fig. 5 and Table 3) suggests that slip on the fault separating these blocks did not juxtapose rocks with significantly different low-temperature thermal histories. Hence, the two blocks can be treated as one for interpreting the thermochronometric data.

2.4.2.2. Apatite. Apatite grains from six samples were difficult to analyze with high precision using traditional fission-track methods due to low U concentrations, which in turn yield low track density (Table 3). In addition, primary fluid inclusions in apatite were often abundant, making it difficult at times to unambiguously differentiate them from tracks, reducing the number of grains and overall tracks possible to count. This factor would lead to anomalous, old apatite ages. Despite these problems, we report the apatite data here for completeness.

The fission-track ages of apatite (3.3–10.3 ppm U) range from 7.2±2.6 to 12.5±4.6 (2σ) Ma (mean 10.4±4.1 Ma). These ages have no clear trend with depth (Table 3), and several are greater than either titanite (23–63 ppm U) or zircon (99–599 ppm U). The problems encountered with the fluid inclusions suggest that the apatite results have limited use for defining the thermal history of Atlantis Bank. The youngest apatite age of 7.2±2.6 Ma (sample #1077),

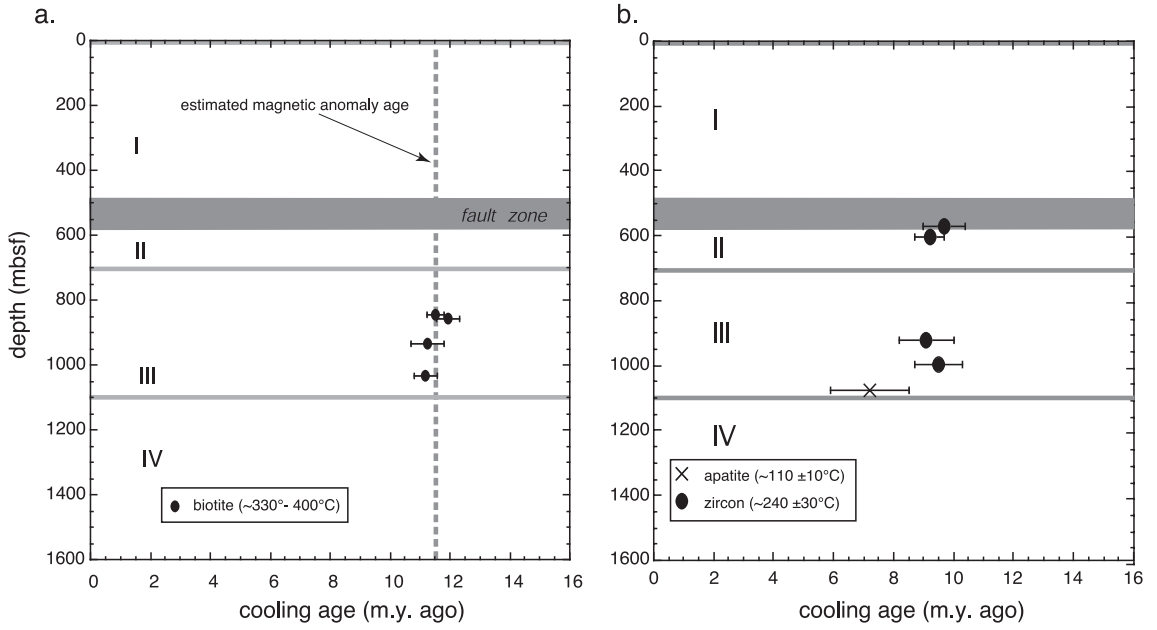

Fig. 5. Intermediate and low temperature history (T~365–110°C): (a) Plot of depth (meters below sea floor) versus $^{40}Ar/^{39}Ar$ cooling age for biotite samples from Hole 735B. Estimated magnetic anomaly age shown as dashed grey line. Errors are ±2σ (shown as bars) and represent standard analytical error. (b) Plot of depth (meters below sea floor) versus cooling age for titanite, zircon, and apatite fission track samples. Errors are ±2σ. Concordance of zircon and titanite FT ages down hole indicate rapid cooling below ~240°C by 9 Ma. Apatite ages, although of poor quality, suggest cooling in the same event.

Table 3
Fission-track analytical results

Sample number	Number of grains dated	$\rho_s \times 10^6$ (t/cm^2)	$\rho_i \times 10^7$ (t/cm^2)	$\rho_d \times 10^5$ (t/cm^2)	Central age (Ma) ($\pm 1\sigma$)	$P(\chi)^2$ (%)	Uranium content (ppm)
Sphene							
279	20	0.08 (77)	0.12 (583)	2.577 (4634)	7.4 (0.9)	>99	63
606	20	0.04 (54)	0.54 (333)	2.582 (4634)	9.1 (1.3)	>99	28
1430	20	0.04 (43)	0.46 (237)	2.587 (4634)	10.2 (1.7)	>99	23
Zircon							
571	15	1.06 (324)	1.07 (1647)	2.616 (4634)	9.7 (0.6)	96	533
606	20	1.11 (1023)	1.21 (5542)	2.615 (4634)	9.1 (0.3)	96	599
920	20	0.18 (153)	0.2 (831)	2.622 (4634)	9.1 (0.8)	>99	99
996	11	0.6 (210)	0.62 (1094)	2.625 (4634)	9.5 (0.7)	>99	308
Apatite							
865	30	0.035 (46)	0.074 (967)	14.1 (4582)	11.1 (1.7)	>98	6.5
920	30	0.015 (22)	0.037 (555)	14.2 (4582)	9.2 (2.0)	>99	3.3
955	30	0.048 (32)	0.090 (605)	14.3 (4582)	12.5 (2.3)	>99	7.9
1040	22	0.055 (39)	0.012 (848)	14.6 (4582)	11.1 (1.8)	>99	10.3
1077	32	0.035 (31)	0.016 (1042)	14.8 (4582)	7.2 (1.3)	>99	9.9
1430	20	0.016 (12)	0.037 (262)	14.8 (4582)	11.2 (3.3)	>99	3

ρ_s—spontaneous track density, ρ_i—induced track density (reported induced track density is twice the measured density). Number in parenthesis is the number of tracks counted for ages and fluence calibration. ρ_d—track density in muscovite detector covering CN-5 (10 ppm); reported value determined from interpolation of values for detectors covering standards at the top and bottom of the reactor packages (fluence gradient correction). S.E.=standard error, $P(\chi)^2$=chi-squared probability, zeta=377±10 for zircon; 435.1±5 for sphene, 330±10 for apatite, $\lambda_d = 1.551 \times 10^{-10}$ year^{-1}, g=0.5.

however, is based on 32 single-grain ages, from grains with reasonable U concentrations, and may approach the time when final temperatures for all samples were less than ~110°C. This age is used later in estimating the low-temperature cooling history of Block III (see below).

3. Discussion and implications

The thermal history of lower oceanic crust recorded by samples collected in situ from Hole 735B provides an unprecedented opportunity to study the timing and rate of heat loss at the very slow spreading SW Indian Ridge. These data represent the first comprehensive set of thermochronometric analyses in oceanic crust. In the discussion below, we attempt to place the data presented in context of the structural history of Atlantis Bank and, more generally, a very slow spreading mid-ocean ridge environment.

Emplacement of the felsic veins drilled in Hole 735B is estimated at 11.93±0.14 Ma based on U–Pb analyses of zircon. This crystallization age is slightly older than the 'crustal age' implied from magnetic data gathered over Hole 735B, which indicate magnetization ~11.5–11.8 Ma. ^{40}Ar/^{39}Ar analyses of biotite give plateau ages of ~11.42±0.21 Ma, implying rapid cooling to temperatures below 330–400°C. Fission-track ages from titanite, zircon, and apatite overlap within respective errors. Using the best quality fission-track data from the analyzed zircon yielded mean ages of ~9.35±1.2 Ma, indicating that the gabbros retained temperatures up to 200°C at least 2.5 m.y. off axis.

3.1. Cooling of lower oceanic crust

Much attention has been paid to the cooling of oceanic lithosphere as a mechanism of heat dissipation from the mantle to produce variations in the thermal structure and therefore rheology, variation in the depth of ocean crust with age, and in the generation of marine magnetic anomalies. The data presented here can be used to place constraints on the

temperature–time (T–t) profile for slow spreading crust to compare with existing models for the thermal evolution of oceanic lithosphere.

Hole 735B sits atop Atlantis Bank, 93 km from the SW Indian Ridge axis, and 18 km east of the present-day Atlantis II transform. At the time of accretion, the Atlantis Bank gabbros are interpreted as having been generated at the northern inside corner high of the paleo-SW Indian Ridge [10]. Theoretical modeling [35] and geophysical observations (e.g. [36]) indicate that the least magmatic portions of slow-spreading ridge segments are at segment ends, where the crust tends to be thin. The lithosphere is thick, and brittle deformation and fault throw maximized in these segments [37,38]. The tectonic setting of inside corners is characterized by shallow water depths, elevated residual mantle Bouguer anomalies suggesting dynamically supported topography and thinner crust, and more widely spaced and larger throw normal faults, with few volcanic features. Dredging and drilling on inside-corner highs along the mid-Atlantic and SW Indian ridges confirm the presence of exposed lower crustal gabbro and peridotite.

Indirect estimates of the original overburden above and the initial crustal thickness at Atlantis Bank and Hole 735B are made from several types of information. Alteration pressure estimates between 90 and 100 MPa, based on a combination of fluid inclusion studies and isotopic analyses of veins from 350 mbsf in Hole 735B, suggest that the sample was originally ~2 km below sea floor [39]. More recent fluid inclusion pressure estimates from the upper 500 m in Hole 735B [14] suggests entrapment pressures of ~700 bars for fluids at temperatures between 400 and 500 °C, implying roughly 2–2.4 km of gabbroic overburden, when the fluids were trapped. Together, these data suggest that the current top of Atlantis Bank was originally some 2.0–2.5 km below the sea floor, prior to denudation by detachment faulting. As Hole 735B is 1500 m deep, the original crustal thickness was therefore at least 3.5–4 km. Robinson [40] calculated Na_8 compositions and predicted a melt thickness of ~3±1 km for dredged basalt from the conjugate to Atlantis Bank north of the SWIR. These estimates equate with REE inversions of the same samples and an estimated melt thickness of 3.0±1.5 km at 735B [40]. The best estimate therefore of the initial overburden above rocks from Block III in Hole 735B (i.e. >700 mbsf) for the purposes of the modeling studies (below) is 3.0±0.5 km, with an initial crustal thickness at this site of ~3.5±1 km.

To investigate the nature of cooling of the crust, we calculated a 2-D finite difference, plate-cooling model for the oceanic lithosphere [41]. A 40-km-long ridge-parallel section of the upper 20 km of the oceanic lithosphere was modeled, assuming a constant temperature (0 °C) upper boundary condition and a zero temperature gradient boundary condition ($dT/dx=0$) at the edges. Temperature at the base of the plate is predicted from the plate-cooling model. A 4-km-thick crust was included, assuming a density of 2900 kg/m^3, specific heat capacity 1000 J/kg/K, and thermal conductivity 2.2 W/m/K, above the mantle with a density of 3300 kg/m^3, specific heat capacity 1260 J/kg/K, and thermal conductivity of 3.15 W/m/K. Cooling ages from the spectrum of thermochronometers used in this study are plotted against estimated blocking or annealing temperatures for Block III in Hole 735B (700–1100 mbsf).

Results of the plate-cooling model combined with the thermochronometric data from Block III are shown in Fig. 6a. Gabbroic rocks drilled at Hole 735B follow a cooling path that initially approximates exponential decay. Initial cooling rates were high, with an average of ~800 °C/m.y. for the first 500,000 years. With time, these rates decreased gradually to 75 °C/m.y. The data are consistent with a model involving conductive cooling of the sampled crust, initially buried to 2–3 km depth. However, the analyzed samples shown in Fig. 6a were collected between ~700 m and 1100 mbsf, and the data are therefore not consistent with a simple conductive cooling history for rocks at this depth. The low-temperature thermochronometric data (FT analyses of zircon and apatite) are not consistent with these predictions and record anomalously high temperatures between ~240 and 110 °C for crust 700 mbsf at ~8–10 Ma (i.e. 2–4 m.y. off axis). More sophisticated models, which include the influence of hydrothermal circulation and/or crustal accretion at the ridge axis, predict lower temperatures for this time and therefore cannot account for these high temperatures [42,43].

We investigate two models that account for the protracted low-temperature cooling history recorded in the rocks from Hole 735B (Fig. 6b). Both include 1.8 km of denudation via detachment faulting using a constant rate of vertical advection for a 20-km-wide

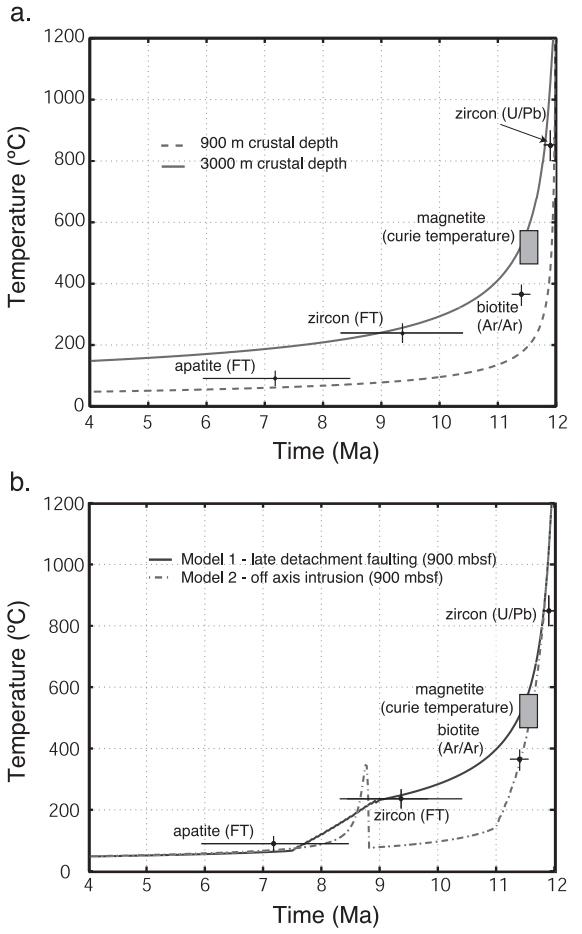

Fig. 6. 2-D temperature-cooling age (time) plot showing data from Block III, Hole 735B for the spectrum of minerals/thermochronometers. (a) Cooling curves derived for a simple plate-cooling model for oceanic lithosphere [41], which defines the initial temperature structure and basal temperature through time. Cooling curves are shown for two initial crustal depths (900 and 3000 m). Data from samples collected above 900 mbsf clearly record anomalously high temperatures. (b) Model curves for two scenarios that can account for the thermochronometric data in (a). Model 1: temperature evolution for a sample from 3000 mbsf denuded to 900 mbsf by late detachment faulting at 8–9 Ma. Model 2: temperature evolution for a sample from 3000 mbsf denuded to 900 mbsf by detachment faulting 11–11.9 Ma, followed by heating due to an off-axis (or asymmetric) magmatic event (the emplacement of a 2-km-thick sill) at 8–9 Ma.

block. Model 1 (solid curve) infers late-stage detachment faulting from 9 to 7.5 Ma and denudation at 1.2 km/m.y. Model 2 (dashed curve) includes denudation from 11.9 to 11 Ma (at 2 km/m.y.) and includes the effect of a laterally continuous, 2-km-thick sill emplaced instantaneously off axis at ~9 Ma.

Model 1 requires detachment faulting and associated denudation of the crust to take place after rocks from 2 to 3 km depth cooled below 240±30°C (FT annealing temperature for zircon) (Fig. 6b) and faithfully records a conductive cooling history. This explanation seems unlikely, as it requires detachment faulting to have occurred at ~9 Ma, 3 m.y. after crust formation, some 20–24 km off the ridge axis. Based on analogies with oceanic core complexes along the mid-Atlantic Ridge, detachment faulting is thought to occur at depth within the axial valley and cease as the crust passes through the rift valley wall [44,45]. The present-day axial valley of the SWIR at this locality is only 9–10 km wide (~1.1 Ma), but it is possible that the axial valley was considerably wider at 12 Ma, possibly a consequence of ridge reorientation due to transtension [46]. If the observed thermal anomaly relates to late detachment faulting, slip on the detachment fault system would have occurred significantly outside the axial valley.

Model 2 implies that crust in the vicinity of Hole 735B suffered off-axis magmatic activity (or asymmetric intrusion) 8.5–9 Ma that caused anomalous reheating of the crust above the annealing temperature for fission tracks in zircon (Fig. 6b). Although this explanation seems poorly constrained, it is supported by several observations. Changes in relative plate motion between 19.5 and 7.5 Ma [9,10,46] put the Atlantis II transform in transtension, with the postulated magmatic event a consequence of that plate reorganization. Even today, bathymetric and dive data indicate a young/active volcanic edifice along the eastern transform valley wall, ~30 km south of the present-day ridge axis [10]. Natland and Dick [47] suggest, based on igneous stratigraphy, the cyclic character of gabbro composition, and the nature of faults cutting core from Hole 735B, that the lower crust may have been thickened by asymmetrical intrusion at or beyond the rift valley wall. In addition, Shinkai 6500 dive observations indicate that the crust–mantle boundary beneath the northern end of Atlantis Bank is exposed at 4.5-km water depth. The present crustal thickness, ≥3.5 km, when combined with the thickness removed by detachment faulting, implies an initial crustal thickness significantly greater (~5.5 km) than other estimates. This

apparent over-thickened crust might be the result of off-axis magmatism.

A combination of the temperature–time and estimated spreading rate data allows calculation of the relative position of a block of ocean crust, and its thermal state, leading to inferences regarding heat loss versus position with respect to the ridge axis and changes in crustal rheology with time. Inferences about the intermediate temperature thermal history of samples from Hole 753B are made from the form of $^{40}Ar/^{39}Ar$ age spectra [4]. During cooling following crystallization, closure temperatures for argon in biotite are normally taken to be between 350 and 280 °C, for cooling rates between 5 and 100 °C/m.y. The estimated cooling rates at Atlantis Bank exceed those stated above (i.e. ~100–800 °C/m.y.). Revised estimates of closure temperatures based on mineral composition and cooling rate are calculated (365±35 °C for biotite) and discussed above.

In the case of crust drilled in Hole 735B, the majority of initial heat content of the crust (~70%) is lost within 0–6 km of the ridge axis, for a temperature range between ~1250 and <400 °C (the difference between the liquidus temperature of gabbro at low pressure and biotite closure temperature), in roughly 500,000–600,000 years. Based on the current configuration of the neovolcanic zone, rift valley wall, and ridge-transform intersection, the rift valley wall emerges from the valley ~4.3 km (nominally 500,000 years) from the zone of active magmatism [10]. The data shown in Fig. 6 suggest that beyond this position, roughly 30% of the magmatic heat budget remains and is lost tens of kilometers away from the ridge, up to several million years off axis. This has important implications for thermal models of the oceanic lithosphere. The influence of hydrothermal circulation at the ridge axis predicts much lower temperatures for the upper lithosphere [41], suggesting that a hydrothermal system either influenced the uppermost crust within the rift valley or played no significant role outside the region. In addition, these data give an idea of the rate of change in plate strength, as the material generated at the ridge passes through temperatures down to 350 °C and is well below the brittle-plastic transition within 500,000 years. They are consistent with recent microearthquake studies showing seismic activity distributed throughout the crust and into the upper mantle within the median valley along the Mid-Atlantic Ridge [48,49], implying a near-axis brittle lower crust in this setting.

3.2. Magnetic anomaly and emplacement ages of gabbroic crust

The primary location of crustal magnetization has classically been considered the volcanic upper crust [50], yet the rocks exposed on Atlantis Bank are denuded subvolcanic (lower) crust and upper mantle with well-defined sea-surface magnetic anomalies [9,10]. Large-scale, sea-surface magnetic surveys over such settings have assumed that these anomalies represent crustal age and are interpreted to estimate the spreading velocity of lithospheric plates. Although the absolute timing of the crystallization of gabbro from Hole 735B is unknown, the relative timing of emplacement of the felsic veins and pods is unambiguous. These minor intrusive bodies everywhere cut gabbro and are both syn- and post-deformation based on crosscutting relationships seen in the core [12]. The U–Pb zircon age from sample #606 therefore represents a minimum crystallization or 'crustal' age for the gabbro of 11.93±0.14 Ma. Based on this age, there was clearly a lag (>50,000–<600,000 years) between the time the felsic vein passed through its solidus at ~850 °C, the time the host rocks passed through their Curie temperature, and the magnetic signature established. The data presented are consistent with, and help quantify, the delayed magnetization of lower crust recognized by rock magnetists ([50] and references therein). At the estimated spreading rate of ~8.5 km/m.y. [9], rocks in Hole 735B cooled below their Curie T, between 500 m and 5 km off axis, most likely near the rift valley wall of the SW Indian Ridge north of Atlantis Bank. We emphasize that sea floor observation taken with precise U–Pb dating, as completed in this study, can provide good constraints on crustal age and help define/constrain magnetic anomaly ages and spreading rates in gabbroic crust from slow and very slow spreading environments.

Acknowledgements

This research used samples and/or data provided by the Ocean Drilling Program (ODP). The ODP is sponsored by the U.S. National Science Foundation

(NSF) and participating countries under management of Joint Oceanographic Institutions (JOI). We would like to acknowledge discussions, comments, and reviews by Henry Dick, Jeff Gee, Greg Hirth, Allegra Hosford, Debbie Kelley, Shari Kelley, Jian Lin, Hans Schouten, and Maurice Tivey. Each contributed to a different aspect of the paper. None, however, should be held to the conclusions presented, as they are the sole responsibility of the authors. Reviews by Mike Bickle, Warren Sharp, Jeff Gee, and an anonymous reviewer both shortened and improved the clarity of the text significantly. Funding for this work came as a JOI/USSSP post-cruise award to John. ***[BW]***

References

[1] J.G. Sclater, B. Parsons, C. Jaupart, Oceans and continents: similarities and differences in the mechanisms of heat loss, J. Geophys. Res. 86 (1981) 11,522–11,535.

[2] C.A. Stein, S. Stein, Constraints on hydrothermal heat flux through the oceanic lithosphere from global heat flow, J. Geophys. Res. 99 (1994) 3081–3095.

[3] J. Gee, W.P. Meurer, Slow cooling of middle and lower crust inferred from multi-component magnetizations of gabbroic rocks from the mid-Atlantic Ridge south of the Kane fracture zone (MARK) area, J. Geophys. Res. 107 (2002) doi: 1029/2000JB000062.

[4] I. McDougall, T.M. Harrison, Geochronology and Thermochronology by the $^{40}Ar/^{39}Ar$ Method, 2nd ed., Oxford Univ. Press, New York, 1999, 212 pp.

[5] P.F. Green, I.R. Duddy, G.M. Laslett, K.A. Hegarty, A.J.W. Gleadow, J.F. Lovering, Thermal annealing of fission tracks in apatite. Qualitative modeling techniques and extensions to geological time-scales, Chem. Geol. 79 (1989) 155–182.

[6] D.A. Foster, B.P. Kohn, A.J.W. Gleadow, Sphene and zircon fission track closure temperatures revisited: empirical calibrations from $^{40}Ar/^{39}Ar$ diffusion studies of K-feldspar and biotite, Int. Workshop Fission Track Dating (Gent), 1996, p. 37.

[7] R. Yamada, T. Tagami, S. Nishimura, H. Ito, Annealing kinetics of fission tracks in zircon: an experimental study, Chem. Geol. 122 (1995) 249–258.

[8] D.A. Foster, B.E. John, Quantifying tectonic exhumation in an extensional orogen with thermochronology: examples from the southern Basin and Range Province, in: U. Ring, M.T. Brandon, G.S. Lister, S.D. Willett (Eds.), Exhumation Processes: Normal Faulting, Ductile Flow and Erosion, Geol. Soc. London Spec. Publ. 154 343–364.

[9] A. Hosford, M. Tivey, T. Matsumoto, H. Dick, H. Schouten, H. Kinoshita, Crustal magnetization and accretion at the Southwest Indian Ridge near the Atlantis II fracture zone, 0–25 Ma, J. Geophys. Res. 108 (2003) doi: 10.1029/2001JB00064.

[10] H.B.J. Dick, H. Schouten, P.S. Meyer, D.G. Gallo, H. Berg, R. Tyce, P. Patriat, K. Johnson, J. Snow, A. Fisher, Tectonic evolution of the Atlantis II Fracture Zone, Proc. Ocean Drill. Program Sci. Results 118 (1991) 359–398.

[11] M. Cannat, Plastic deformation at an oceanic spreading ridge; a microstructural study of the Site 735 gabbros (Southwest Indian Ocean), Proc. Ocean Drill. Program Sci. Results 118 (1991) 399–408.

[12] H.J.B. Dick, J.H. Natland, D.J. Miller, Shipboard Science Party, Proc. Ocean Drill. Program, Initial Rep. 176. College Station, TX (1999), CD-ROM.

[13] H.J.B. Dick, et al., A long in-situ section of lower oceanic crust: results of ODP Leg 176 drilling at the Southwest Indian ridge, Earth Planet. Sci. Lett. 179 (2000) 31–51.

[14] D.S. Kelley, G.L. Früh-Green, Volatile lines of descent in submarine plutonic environments: insights from stable isotope and fluid inclusion analyses, Geochim. Cosmochim. Acta 65 (2001) 3325–3346.

[15] H.B.J. Dick, P.S. Meyer, S. Bloomer, S. Kirby, D. Stakes, C. Mawer, Lithostratigraphic evolution of an in-situ section of oceanic layer 3, Proc. Ocean Drill. Program Sci. Results 118 (1991) 439–540.

[16] D. Stakes, C. Mevel, M. Cannat, T. Chaput, Metamorphic stratigraphy of Hole 735B, Proc. Ocean Drill. Program Sci. Results 118 (1991) 153–180.

[17] P.T. Robinson, H.J.B. Dick, R. Von Herzen, Metamorphism and alteration in oceanic layer 3: Hole 735B, Proc. Ocean Drill. Program Sci. Results 118 (1991) 541–552.

[18] S.A. Swift, H. Hoskins, R.A. Stephen, Seismic stratigraphy in a transverse ridge, Atlantis II fracture zone, Proc. Ocean Drill. Program Sci. Results 118 (1991) 219–226.

[19] S.C. Cande, D.V. Kent, Revised calibration of the geomagnetic polarity time scale for the Late Cretaceous and Cenozoic, J. Geophys. Res. 100 (1995) 6093–6095.

[20] S. Allerton, M.A. Tivey, Magnetic polarity structure of the lower oceanic crust, Geophys. Res. Lett. 28 (2001) 423–426.

[21] W. Compston, J. Kirschvink, A. Zhang, C. Ma, Zircon U–Pb ages for the Early Cambrian time scale, J. Geol. Soc. Lond. 149 (1992) 171–184.

[22] I.S. Williams, U–Th–Pb geochronology by ion microprobe, in: M.A. McKibben, et al (Ed.), Applications of microanalytical techniques to understanding mineralization processes, Reviews in Economic Geology 7, (1998) 1–35.

[23] F. Tera, G.J. Wasserburg, U–Th–Pb systematics in three Apollo 14 basalts and the problem of initial Pb in lunar rocks, Earth Planet. Sci. Lett. 14 (1972) 281–304.

[24] J. Lee, I. Williams, D. Ellis, Pb, U and Th diffusion in natural zircon, Nature 390 (1997) 159–162.

[25] T.L. Spell, I. McDougall, A.P. Doulderis, Cerro Toledo Rhyolite, Jemez Volcanic field, New Mexico: $^{40}Ar/^{39}Ar$ geochronology of eruption between two caldera forming events, Geol. Soc. Amer. Bull. 108 (1996) 1549–1566.

[26] A.J.W. Gleadow, J.F. Lovering, Thermal history of granitic rocks from western Victoria: a fission-track dating study, Geol. Soc. Aust. J. 25 (1978) 323–340.

[27] R.J. Scott, D.A. Foster, G.S. Lister, Tectonic implications of rapid cooling of denuded lower plate rocks from the Buckskin–Rawhide metamorphic core complex, west-central Arizona, Geol. Soc. Amer. Bull. 110 (1998) 588–614.

[28] P.G. Fitzgerald, A.J.W. Gleadow, Fission track geochronology, tectonics and structure of the Transantarctic Mountains in northern Victoria Land, Antarctica, Chem. Geol. 73 (1988) 169–198.
[29] A.J.W. Gleadow, I.R. Duddy, P.F. Green, J.F. Lovering, Confined fission track lengths in apatite: a diagnostic tool for thermal history analysis, Contrib. Mineral. Petrol. 94 (1986) 405–415.
[30] C.W. Naeser, Fission track dating and geologic annealing of fission tracks, in: E. Jager, J.C. Hunziker (Eds.), Lectures in Isotope Geology, Springer-Verlag, New York, 1979, pp. 154–169.
[31] A.J. Hurford, P.F. Green, The zeta age calibration of fission-track dating, Chem. Geol. 41 (1983) 285–317.
[32] P. Green, A new look at statistics in fission track dating, Nucl. Tracks 5 (1981) 77–86.
[33] R. Galbraith, On statistical methods in fission track counts, Math. Geol. 13 (1981) 471–488.
[34] R.F. Galbraith, G.M. Laslett, Statistical models for mixed fission track ages, Nucl. Tracks Radiat. Meas. 21 (1993) 459–470.
[35] D.W. Sparks, E.M. Parmentier, J. Phipps-Morgan, Three-dimensional mantle convection beneath a segmented spreading center; implications for along-axis variations in crustal thickness and gravity, J. Geophys. Res. 98 (1993) 21,977–21,995.
[36] J. Lin, G.M. Purdy, H. Schouten, J.-C. Sempere, C. Zervas, Evidence from gravity data for focused magmatic accretion along the Mid-Atlantic Ridge, Nature 344 (1990) 627–632.
[37] P.R. Shaw, J. Lin, Causes and consequences of variations in faulting style at the Mid-Atlantic Ridge, J. Geophys. Res. 98 (1993) 21,839–21,851.
[38] J. Escartin, G. Hirth, B. Evans, Effects of serpentinization on the lithospheric strength and the style of normal faulting at slow-spreading ridges, Earth Planet. Sci. Lett. 151 (1997) 181–189.
[39] D.A. Vanko, D.S. Stakes, Fluids in ocean layer 3: evidence from veined rocks, Hole 745B, Southwest Indian Ridge, Proc. Ocean Drill. Program Sci. Results 118 (1991) 181–215.
[40] C.J. Robinson, Mantle melting and crustal generation at the very slow spreading Southwest Indian Ridge; unpublished PhD dissertation, University of Cambridge, 1998, 241 pp.
[41] C.A. Stein, S. Stein, A model for the global variation in oceanic depth and heat flow with lithospheric age, Nature 359 (1992) 123–129.
[42] T.J. Henstock, A.W. Woods, R.S. White, The accretion of oceanic crust by episodic sill intrusion, J. Geophys. Res. 98 (1993) 4143–4161.
[43] J. Phipps Morgan, Y.J. Chen, The genesis of oceanic crust: magma injection, hydrothermal circulation, and crustal flow, J. Geophys. Res. 98 (1993) 6283–6297.
[44] D.K. Blackman, J.R. Cann, B. Janssen, Origin of extensional core complexes: Evidence from the Mid-Atlantic Ridge at Atlantis fracture zone, J. Geophys. Res. 103 (1998) 21315–21333.
[45] B.E. Tucholke, J. Lin, M.C. Kleinrock, Megamullions and mullion structure defining oceanic metamorphic core complexes on the Mid-Atlantic Ridge, J. Geophys. Res. 103 (1998) 9857–9866.
[46] A.G. Baines, M.J. Cheadle, H.J.B. Dick, A.H. Scheirer, B.E. John, N.J. Kusznir, T. Matsumoto, Mechanism for generating the anomalous uplift of oceanic core complexes: Atlantis Bank, southwest Indian Ridge, Geology 31 (2003) 1105–1108.
[47] J.H. Natland, H.J.B. Dick, Stratigraphy and composition of gabbros drilled in Ocean Drilling Program Hole 735B, Southwest Indian Ridge: A synthesis of geochemical data, Proc. Ocean Drill. Program Sci. Results 176 (2002) 1–69.
[48] C. Wolfe, G.M. Purdy, D.R. Toomey, S.C. Solomon, Microearthquake characteristics and crustal velocity structure at 29 N of the Mid-Atlantic Ridge: the architecture of a slow-spreading segment, J. Geophys. Res. 100 (1995) 24449–24472.
[49] F. Tilmann, L. Planert, E. Flueh, T. Reston, W. Weinrebe, Local seismicity of the slow spreading Mid-Atlantic Ridge: median valley earthquakes shallow towards the segment end, Geophys. Res. Abstr., 5 (2003) 05263.
[50] C.G.A. Harrison, Marine magnetic anomalies—the origin of the stripes, Annu. Rev. Earth Planet. Sci. 15 (1987) 505–543.